The effect of Reynolds number on the flow around the T106C very high lift low pressure turbine linear cascade

Antoine Dufau, Julien Marty, Estelle Piot, Daniel Man

▶ **To cite this version:**

Antoine Dufau, Julien Marty, Estelle Piot, Daniel Man. The effect of Reynolds number on the flow around the T106C very high lift low pressure turbine linear cascade. ETC 15 - European Turbomachinery Conference, Apr 2023, Budapest, Hungary. hal-04099296

HAL Id: hal-04099296
https://hal.science/hal-04099296

Submitted on 16 May 2023

HAL is a multi-disciplinary open access archive for the deposit and dissemination of scientific research documents, whether they are published or not. The documents may come from teaching and research institutions in France or abroad, or from public or private research centers.

L'archive ouverte pluridisciplinaire **HAL**, est destinée au dépôt et à la diffusion de documents scientifiques de niveau recherche, publiés ou non, émanant des établissements d'enseignement et de recherche français ou étrangers, des laboratoires publics ou privés.

THE EFFECT OF REYNOLDS NUMBER ON THE FLOW AROUND THE T106C VERY HIGH LIFT LOW PRESSURE TURBINE LINEAR CASCADE

Antoine Dufau[1] - *Julien Marty*[2] - *Estelle Piot*[3] - *Daniel Man*[1]

[1]Safran Aircraft Engines, Moissy-Cramayel, France
[2]ONERA, Meudon, France
[3]ONERA/DMPE, Université de Toulouse, F-31055 Toulouse, France

ABSTRACT

Low pressure turbines flows are highly dependent on the boundary layer transition and laminar separation because of the low Reynolds number environment and the high blade loading. In the case of a laminar separation, the transition of the shear layer is triggered by instabilities and a recirculation zone appears near the wall. This phenomenon is known as a laminar separation bubble. Depending on its characteristics, the laminar separation bubble can be categorized as open, long or short. Some experiments performed at the von Karman Institute investigated the effect of Reynolds number on the topology of the separation bubble over the suction side of the very high lift T106C blade. In a previous work, the authors have performed a high fidelity simulation on this configuration at the Reynolds number of 100 000 and shown some discrepancies with the experiments. In order to deepen this study, three others simulations at three higher Reynolds numbers have been performed. Thus a wider comparison between QDNS (Quasi Direct Numerical Simulation) and the experiments is proposed in this paper. Moreover, the simulations give a more detailed descriptions of the effect of Reynolds number on the laminar separation bubble. Finally, we discuss the flow predicted by RANS simulations by making a comparison with the flow computed with the QDNS with the intention of validating the γ-$\widetilde{Re}_{\theta t}$ transition model on low pressure turbine cases.

KEYWORDS

LAMINAR SEPARATION BUBBLE, LP TURBINE, TRANSITION, QDNS, RANS, T106C

NOMENCLATURE

H_i	boundary layer shape factor	δ	boundary layer thickness
k	turbulent kinetic energy	δ_1	displacement thickness
M	Mach number	θ	momentum thickness
P	pressure	τ_w	skin friction coefficient
Re	Reynolds number	$_{is}$	isentropic
T	temperature	$_0$	total
α	flow angle	$_s$	static
β	blade stagger angle	$_1$	upstream
γ	intermittency	$_2$	downstream

 Copyright © by the Authors
Downloaded from www.euroturbo.eu

INTRODUCTION

The low-pressure turbine of a turbofan engine can operate at a low Reynolds number especially for cruise conditions at high altitude. Consequently, the boundary layer over the airfoils can be laminar on a large part of the suction side. As the low-pressure turbine is responsible for 30% of the engine weight, a common engine design tendency is the reduction of turbine blade number. An increase of the pitch between the blades leads to an increase of the blade loading usually defined by the Zweifel coefficient. The main consequence of a high blade loading is the presence of a high adverse pressure gradient over the suction side that may lead to the separation of the still laminar boundary layer. The evolution of the separated shear layer is then closely linked to its laminar-turbulent transition. Different parameters influence the topology of the laminar separation bubble such as the Reynolds number or the free-stream turbulence intensity. Indeed, for a low Reynolds number, the separation bubble can be open, meaning that there is no reattachment of the separated shear layer. When the Reynolds number increases, the separation bubble may be closed so the separated shear layer reattaches before the trailing edge. This closed bubble is categorized as long or short depending on the static pressure plateau length and the generated losses. The switch from short bubble to long bubble is called the bursting. There are several definitions of a short versus long bubble. One is when the bubble length is quickly increasing for a small change of aerodynamic conditions (Gaster, 1967). Marxen and Henningson (2011) proposed a list of definitions of what distinguish a short bubble from a long one. One of them is that a short bubble does not have an global effect on the flow. Another one is that, for a short bubble, the point of transition and production of turbulent kinetic energy is the location of the pressure recovery.

The T106C linear cascade is an experimental high loaded low-pressure turbine blade cascade studied at the von Karman Institute (Michálek et al., 2012). Experimental measurements have been made for a large range of Reynolds numbers and several turbulent intensities. To the best knowledge, the only flow condition simulated with DNS or QDNS is a Reynolds number of 80,000 and the lowest level of turbulence intensity (0.8%). The three groups of authors that have done this simulation are Hillewaert et al. (2014), Garai et al. (2016) and Alhawwary and Wang (2020). They all have shown similar results and that there are some discrepancies between the high fidelity simulation and the experimental measurements. The isentropic Mach number distribution differs, especially in the laminar separation zone and the favorable pressure gradient part of the suction side. To reduce this, Hillewaert et al. (2014) proposed a slight modification of the geometry by modifying the stagger angle of 1 degree and the inlet flow angle of 2 degree. This modification reduced the differences but it did not remove them entirely. Even more recently, we performed a QDNS of the flow around T106C cascade at the Reynolds number of 100,000 and the lowest level of turbulence intensity (Dufau et al., 2022). Similar discrepancies with the experiments have been highlighted and the modification of the stagger angle resulted again in a better match but a unexplained mismatch remains in the laminar separation zone.

In the conclusion of our last study, one of our hypothesis was that the low Reynolds numbers causes a phenomenon in the experimental facility that the simulation does not capture. Consequently, this paper aims at investigating this hypothesis by performing Quasi Direct Numerical Simulations of the flow around T106C turbine cascade blade for three higher Reynolds numbers : 120,000, 140,000 and 160,000. As in the previous study, the freestream turbulence of the wind tunnel is replicated by adding an injection of synthetic turbulence at the inlet plane with the Synthetic Eddy Method. Moreover, the modifications of the stagger angle of $1^o$and of the incidence angle of 2.3^o have been kept for these new simulations. It should be noted that these modifications are similar to the ones investigated by Hillewaert et al. (2014) . QDNS results are

compared to experimental data in order to investigate the discrepancies already observed at the Reynolds number 80,000 and 100,000 in the literature. The ultimate purpose of our work is to evaluate the γ-$\widetilde{Re}_{\theta t}$ transition model on the T106C configuration. Therefore, we performed an assessment of RANS simulations coupled with γ-$\widetilde{Re}_{\theta t}$ transition model by comparing the flow simulated at the same conditions with the QDNS taken as a reference.

T106C CASCADE : GEOMETRY AND EXPERIMENTS

The geometry chosen for our study is the T106C cascade which is a very high lift low pressure turbine blade cascade. It has been tested experimentally by the von Karman Institute in the S1-C facility in the framework of the European project TATMo (Michálek et al., 2012). The experimental setup is made up of 6 aligned blades. One of the two blades at the center is used for the measurements which have been performed for a range of exit isentropic Reynolds number $Re_{2,is}$ from 80,000 to 250,000 and several level of turbulence intensity Tu from 0.8% to 3.2%. Thanks to the variable density characteristic of the S1-C facility, the exit isentropic Mach number is kept constant at 0.65. The characteristics of the T106C are stated in table 1.

Chord c [mm]	93.01
Pitch to chord ratio [-]	0.95
Aspect ratio [-]	2.4
Blade stagger angle [deg]	30.7
Inlet flow angle α_1 [deg]	32.7
Zweifel coefficient	1.29

Table 1: T106C characteristics

NUMERICAL METHOD

Quasi Direct Numerical Simulations

The term QDNS (Quasi Direct Numerical Simulation) is chosen to describe a DNS-type simulation for which the cell size does not reach the Kolmogorov scale but is small enough to have similar results. It has to be noted that even if we chose to use this term to be more accurate, the simulations of this study are on the same level of discretization as most of the DNS simulations performed on similar configurations in the literature. Some observations on the turbulence resolution are available in Dufau et al. (2022) with power spectral densities.

For this study, four QDNS have been performed with the ONERA in-house code *FastS*. This solver has already been validated with several studies (Dandois et al., 2018; Lugrin et al., 2021; Gleize et al., 2021) and was created from the solver *FLU3M* by adding a python interface and an optimization of the HPC performance based on a hybrid MPI/OpenMP framework. The time scheme used is the second order accurate backward scheme of Gear. The spatial scheme is also of second order. The global time step used for the three simulations is $4.3 \cdot 10^{-7} s$ which equals about 10^{-3} convective time units and leads to a maximal CFL number about 25 in the smallest cells of the grid. The inlet condition is a subsonic inflow condition for which five variables are specified: stagnation pressure, stagnation enthalpy and the three components of the velocity direction unit vector. The outlet condition is a subsonic outflow condition for which the static pressure is specified. As we make the hypothesis of 2.5D flow of a linear cascade, periodic conditions are used in y and z directions. An adiabatic no-slip condition is used at the blade wall. In the experiments with no turbulence grid (No Grid case), the turbulence intensity is about 0.8% near the leading edge. To get closer to the experimental conditions, an injection of

$Re_{2,is}$ [-]	$M_{2,is}$ [-]	$P_{0,1}$ [Pa]	$T_{0,1}$ [K]	α_1 [^{o}]	$P_{s,2}$ [Pa]	β [^{o}]
100,000	0.65	9027.6	299	35	6796.2	1
120,000	0.65	10833.1	299	35	8155.5	1
140,000	0.65	12638.6	299	35	9514.7	1
150,000	0.65	14444.1	299	35	10874.0	1

Table 2: List of the QDNS

synthetic turbulence is done at the inlet of the domain. The method known as SEM (Synthetic Eddy Method) developped by Jarrin et al. (2006) is used to create a map of velocity fluctuations that is injected at the inlet boundary condition. This map is created from the locations of fictive eddies which are moving in a phantom box that surrounds the inlet plane. A modification of the method has been made in order to take account of the periodic boundaries of the inlet plane. Consequently, an issue of non coherent injection at the boundaries of the inlet plane has been avoided. More information about the SEM is given in Dufau et al. (2022).

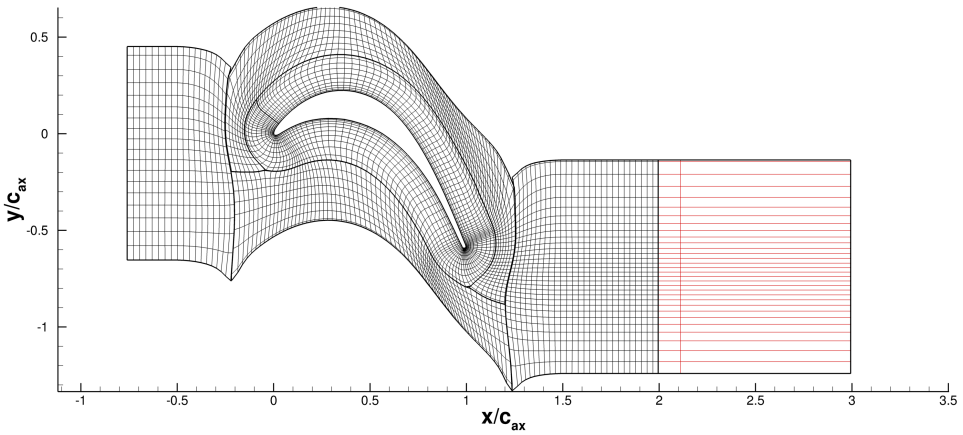

Figure 1: Mesh for QDNS (1 point over 15 in each direction) - Red zone is the buffer zone

As previously stated, for all the simulations, the selected geometry is the experimental blade for which the stagger angle has been modified by $\beta = 1^o$. The mesh used is the same mesh that has been designed for our last study in (Dufau et al., 2022). It is shown in figure 1. The same mesh is used for all four simulations. The mesh is made with one O-type grid around the blade and four H-type grids. Two others H-type grids are used upstream and downstream to extrude the mesh towards the inlet and the outlet planes of the domain. A buffer zone is placed downstream of the mesh in order to cancel the acoustic reflections on the outlet boundary conditions. This buffer zone is an extrusion of the mesh with an expansion ratio of 1.15. No buffer zone has been designed at the upstream part because of the injection of synthetic turbulence. In terms of mesh cells size, the non-dimensional wall cells lengths were fixed to have maximum values fulfilling $x^+ < 10$, $y^+ < 2$ and $z^+ < 5$. Moreover, the maximum expansion ratio has been kept under 1.02. The 2D mesh is extruded along the span direction for 30% of the axial chord. In the previous study, the non span-wise correlation has been verified with the observation Pearson correlation coefficient along a span-wise line in the wake of the blade.

The simulations have been performed for around 200 convective time scales. The end of the transitory state has been considered after 100 convective time scales. So the time average quantities shown in this study have been computed over 100 convective time scales.

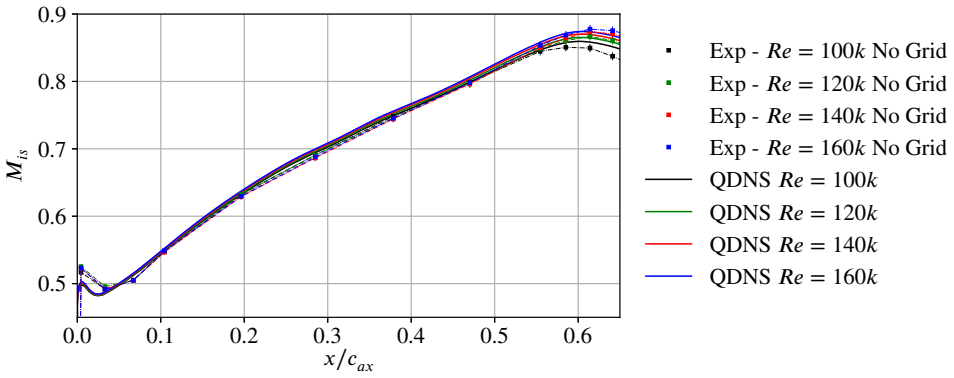

Figure 2: Isentropic Mach Number M_{is} distribution around T106C blade - upstream part of the suction side

Reynolds Averaged Navier-Stokes simulations

RANS simulations has been performed with the ONERA in-house tool *elsA* (Cambier et al., 2013; Plot, 2019). The second order in space upwind scheme of Roe, an implicit time scheme and a scalar LUSSOR implicit method are used. A local time step is fixed with a CFL condition set at 10. The simulations are performed for 40 000 iterations which ensures a reduction of residuals of more than 5 orders of magnitude. Turbulence and transition are modelled by using the $k-\omega$ turbulence model of Wilcox (1988) and the γ-$\widetilde{Re}_{\theta t}$ transition model of Menter et al. (2006). The geometric setup is a 2.5D mesh with periodic boundaries. A 2D mesh of around 82,000 points is extruded on 11 points along span direction. A mesh convergence study has been performed and lead to the following main characteristics: $x^+ < 100$, $y^+ < 1$ and an average of 40 points in the boundary layer thickness.

COMPARISON BETWEEN QDNS AND THE EXPERIMENTS

Figure 2 and figure 3 show the evolution of the isentropic Mach number over the stator blade wall along the upstream and downstream parts of the suction side, respectively. Four Reynolds numbers based on the isentropic exit velocity are plotted for both the QDNS and the experiments. The comparison between experimental data and QDNS results shows a good agreement along the upstream part, proving that the growth of the boundary layer in favorable pressure gradient region is well captured by QDNS if the blade stagger angle is modified as already shown in Dufau et al. (2021) for $Re_{2,is} = 100\ 000$ This evolution of isentropic Mach number is similar to the ones obtained by Hillewaert et al. (2014), Garai et al. (2015) and Alhawwary and Wang (2020), especially concerning the local extremum at the leading edge. Moreover, as in the experiments, the Reynolds number has no effect on this region, the main driving parameters being the incidence and the stagger angles (Dufau et al., 2022).

On the contrary, the Reynolds number influences strongly the isentropic Mach number distribution over the downstream part of the blade, i.e. in the strong adverse pressure gradient region. The same tendency is observed with both the QDNS and the experiments. Indeed, as the Reynolds number increases, the isentropic Mach number rises, showing a higher blade loading. The static pressure plateau is reduced when the onset of the separation occurs later and turbulent reattachment occurs earlier. Nevertheless, the position of the isentropic Mach number peak does not depend on the Reynolds number. In terms of isentropic Mach number peak, the comparison between experimental and numerical data shows that the location predicted by QDNS at 60% of the axial chord is slightly upstream of the experimental location close to 61.6%. However,

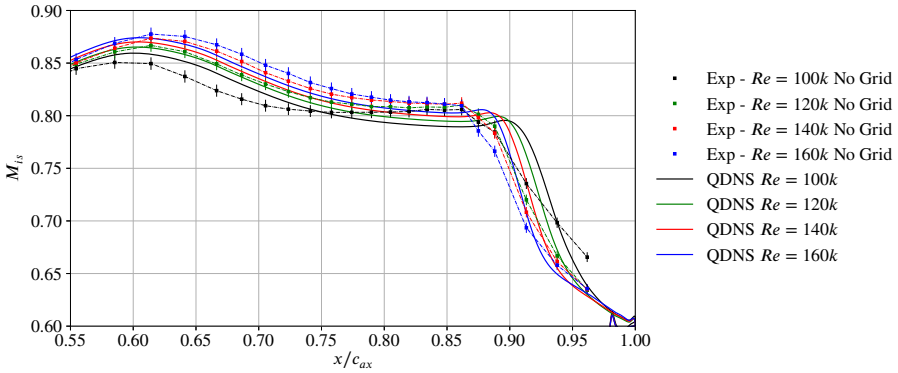

Figure 3: Isentropic Mach Number M_{is} distribution around T106C blade - downstream part of the suction side

the experimental discretization is quite coarse to conclude a mis-match between experiments and QDNS. Moreover, the higher the Reynolds number, the better the agreement, especially the slope of the isentropic Mach number in the region of pressure recovery linked to the boundary layer reattachment. For the three highest Reynolds numbers, the slope is quite brutal in the experiments just as in the QDNS. On the contrary, the Re=100k case exhibits a smoother slope in the experiments while it is again quite brutal in the QDNS. For this Reynolds number, the bubble is probably open in the experiments. Michálek et al. (2012) state that at this Reynolds number the experimental separation bubble is open while it is long at Re=120k. This could explain the difficulties to well predict the flow at lower Reynolds number, as in Hillewaert et al. (2014), Garai et al. (2015) and Alhawwary and Wang (2020). Closer to the trailing edge, the slope of deceleration decreases in QDNS. This effect is also observed in the experiments for the Reynolds numbers higher than 140,000. For Re=120k, as the bubble is longer, this slope amplitude decrease is not observed in the experiments but it could be explained by the lack of probes closer to the trailing edge.

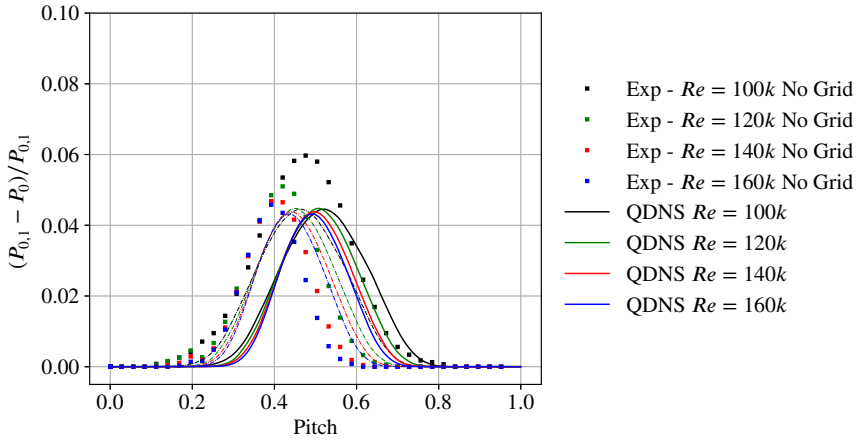

Figure 4: Total pressure deficit distribution in the wake of T106C blade - dashed lines corresponds to distributions with corrected pitch

Figure 4 depicts the total pressure deficit distribution along the pitchwise direction, in the wake of the T106C blade at $0.5c_{ax}$ of the trailing edge, for all investigated Reynolds numbers. The dashed lines represent the same profiles as the solid lines but with a translation in pitch

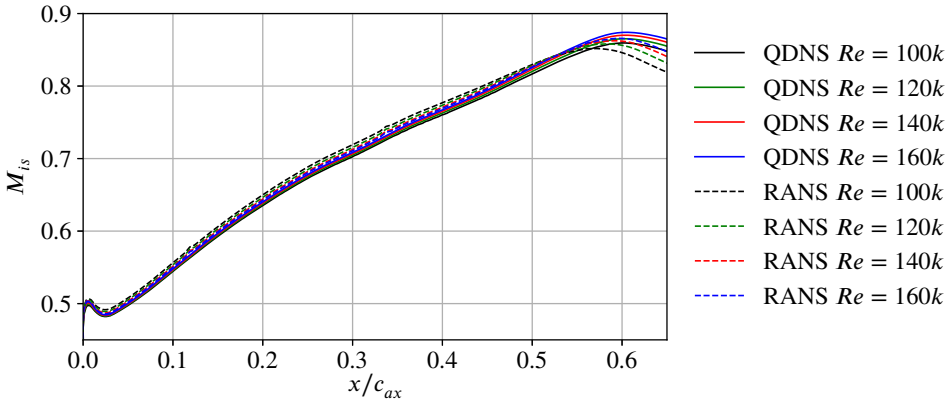

Figure 5: Isentropic Mach Number M_{is} distribution around T106C blade - upstream part of the suction side

to account for the change of stagger angle including both the translation of the position of the trailing edge and the modification of the outlet flow angle. The first observation that can be made is the obvious mismatch between the experiments and QDNS at Re=100k as already described in Dufau et al. (2022). Moreover, the analysis of the experimental data shows that, as the Reynolds number increases, the deficit decreases which means the losses are reduced, and the peak location moves to lower pitch values. The main phenomenon leading to loss reduction is probably the switch from open to long bubble and then from long to short bubble. The increase of the wake peak and width is also observed on the QDNS distributions. However, the difference between the Re=100k and Re=120k cases is much less pronounced in the QDNS compared to the experiments. As shown earlier with the isentropic Mach number, and later with other analysis, this discrepancy comes from the mis-match in terms of bubble topology between experiments (open bubble) and QDNS (long bubble). For higher Reynolds number, the agreement is good between experimental and QDNS results for total pressure deficit levels and the wake thickness is slighly larger in QDNS.

In this comparison between the QDNS and the experiments, it has been shown that the agreement is getting better when the Reynolds number is increased. This is supporting our initial hypothesis that the QDNS might be missing a phenomenon existing in the experiments for the lowest Reynolds numbers. However, the authors consider that the good match for the highest Reynolds number allows to use QDNS as a reference to assess the transition model.

ASSESSMENT OF RANS SIMULATIONS COUPLED WITH γ-$\widetilde{Re}_{\theta t}$ MODEL

Macroscopic analysis

Figures 5 and 6 show the distribution of isentropic Mach number over the upstream part of the T106C wall for all investigated Reynolds numbers, for both RANS and QDNS computations, the latter being taken as references. The evolution in the region characterized by the favorable pressure gradient i.e. the increase of isentropic Mach number differs between RANS and QDNS, the former being higher than the latter, in the first 20% of the axial chord. Then, curves are quite parallel, except for the lowest Reynolds number investigated. Subsequently, this leads to some significant discrepancies from the isentropic Mach number peak. The first one concerns the location of this peak: there is no significant effect of Reynolds number on QDNS results while RANS computations highlight an effect since the location moves downstream when the Reynolds number increases. Quantitatively, the location switches from 57.5%

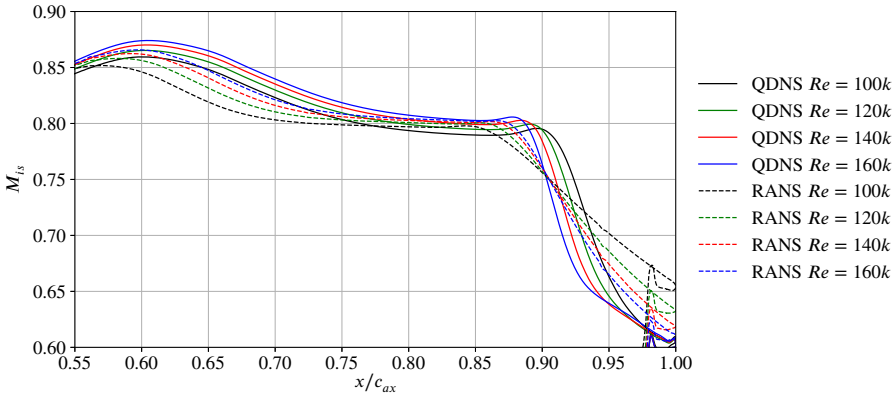

Figure 6: Isentropic Mach Number M_{is} distribution around T106C blade - downstream part of the suction side

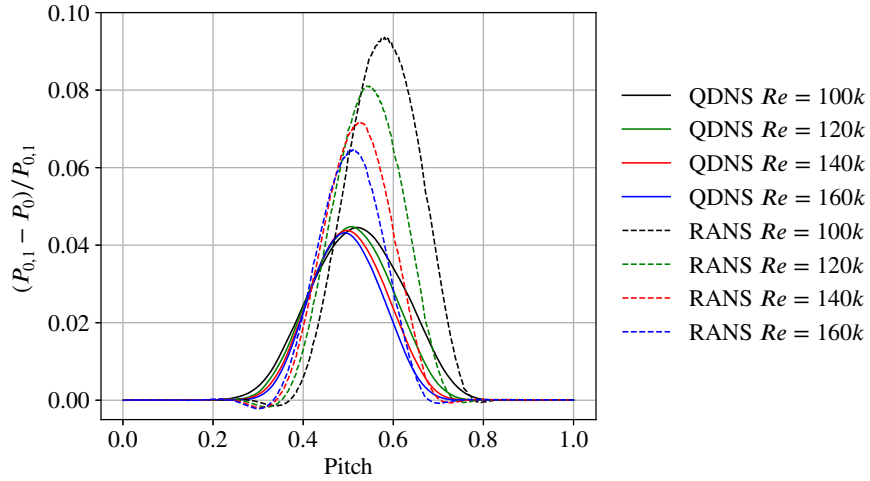

Figure 7: Total pressure deficit distribution in the wake of T106C blade

up to 61% of axial chord.

Once the peak is passed, as shown in Figure 6, RANS and QDNS distributions diverge. The laminar separation occurs earlier for RANS simulations as the plateau of static pressure appears more upstream. The location of the beginning of pressure recovery due to the laminar-turbulent transition differs also. The static pressure recovery is smoother for RANS computations than for QDNS. Moreover, the isentropic Mach number at the trailing edge is highly dependent of the Reynolds number for RANS simulations while it is identical for all the QDNS. By analyzing Figure 3 and Figure 6 for the Re=100k case, RANS results are in better agreement with the experimental data than the QDNS. According to Michálek et al. (2012), the experimental separation bubble is open at $Re_{2,is} = 100\ 000$ so the RANS might also predict an open bubble. For the three higher Reynolds number cases, the experiments seems to be in better agreement with the constant isentropic Mach number at trailing edge observed with the QDNS.

Figure 7 depicts the total pressure loss profile computed in an axial plane downstream of the blade. The main parameters concerning this profile are the level of loss and the location of its maximum and, the thickness of the wake. QDNS results show that the Reynolds number influences mainly on the wake thickness which is reduced as the Reynolds number increases. The

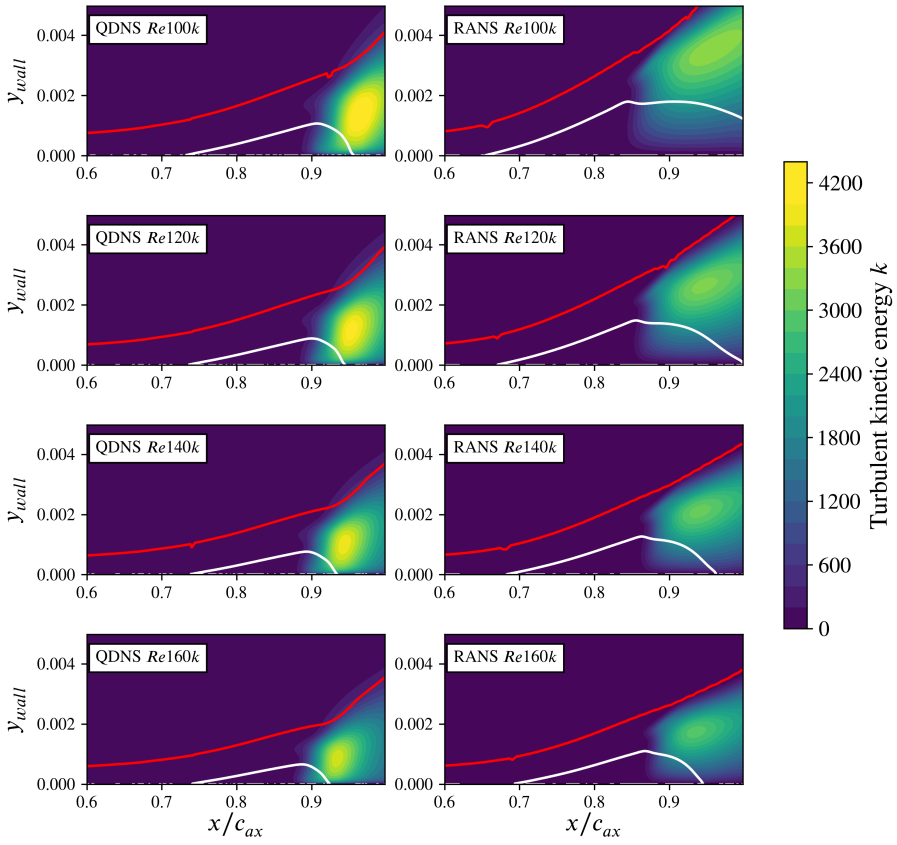

Figure 8: Contours of turbulent kinetic energy k over the downstream part of the suction side of the blade (Red line : Boundary layer thickness δ – White line : Limit of the recirculation zone $u_s = 0$)

location of the loss maximum is slightly modified while the maximum value is quite constant with the Reynolds number. On the contrary, all parameters are significantly dependent on the Reynolds number for the RANS simulation: the wake thickness and the loss level decrease with the rise of Reynolds number. Moreover, the location of the loss maximum moves from 0.52 to 0.44 pitchwise. In the present frame, the left part is linked to the pressure side, and the right one to the suction side. The reduction of the wake thickness appears mainly towards the suction side. This is the footprint of the switch from an open bubble to a closed one. The comparison with the experimental data shows that the change of the wake profile is over-estimated by RANS, especially for Reynolds number higher or equal to 120,000.

Laminar separation bubble

Contours of turbulent kinetic energy over the downstream half of the suction side are depicted in Figure 8. The white represents the boundary of the recirculation zone, $u_s = 0$ where u_s is the streamwise velocity and the red line outlines the boundary layer edge. For both RANS and QDNS, as the Reynolds number increases, the separation point moves downstream while the reattachment one upstream, leading to a smaller bubble in terms of length and thickness. The separation bubble in the QDNS is always closed while it is predicted open for the Re=100k case by the RANS simulation. If we consider the two definitions distinguishing a long from a short bubble, the QDNS seems to predict a short bubble for all Reynolds numbers. Indeed, the

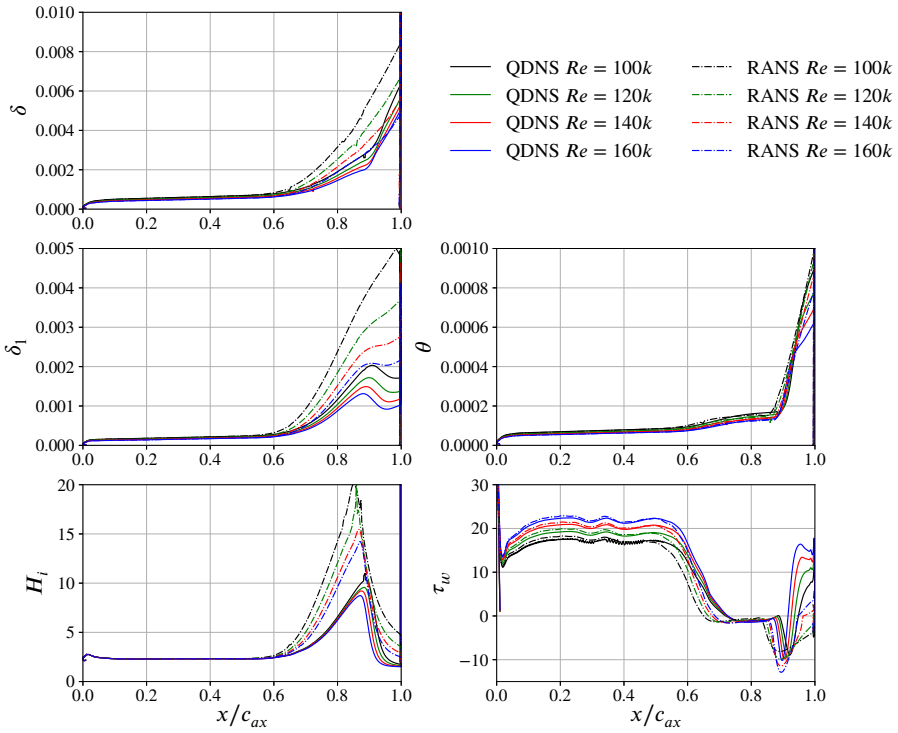

Figure 9: Evolution of boundary layer thickness δ, displacement thickness δ_1, momentum thickness θ, shape factor H_i and skin friction coefficient τ_w on the suction side of T106C blade

bubble length is varying equally when the Reynolds number is decreasing and the location of turbulence production is matching with the end of the recirculation zone. However, according to these definitions, RANS simulations predict a long bubble for the Re=120k case, and a short bubble for the Re=160k case and a bubble close to bursting for the Re=140k case.

The comparison of turbulent kinetic energy (TKE) fields shows that, in RANS computations based on Boussinesq hypothesis, the production of turbulence is clearly insufficient and is responsible for a delay of turbulent reattachment. This statement was already observed in previous studies such as in Bouchard et al. (2021) based on Spalart-Allmaras turbulence model. Moreover, the TKE peak is mainly predicted in the upper part of the laminar separation bubble and the turbulence production follows the streamwise direction as if the convective terms have a higher influence than the diffusive ones. On the contrary, in QDNS results, the turbulence production occurs in a larger part of the bubble thickness and, at the same streamwise location, there is a slope break in the boundary layer thickness evolution. These discrepancies in terms of TKE production explain the divergence between RANS and QDNS results, in terms of bubble topology leading to differences on macroscopic data such as isentropic Mach number and loss profile.

The boundary layer integral thicknesses and shape factor evolution are plotted in Figure 9 along with the skin friction magnitude weighted by the sign of the streamwise component in order to highlight separation with negative value. In the laminar part, RANS and QDNS predict similar skin friction, except for the first twenty percents, where RANS under-predicts the friction. This could be correlated with the different behavior obtained on the isentropic Mach number. The skin friction becomes negative prematurely for RANS computations, confirming that the separation occurs earlier with this approach. Once the separation has occurred, the

level of skin friction is similar between RANS and QDNS. The discrepancies appear in the last part of the separation bubble i.e. after the transition onset. The high turbulence production in QDNS leads to a sudden increase of skin friction. On the contrary, in RANS computations, due to smaller turbulence production, the increase is slower, especially at the lowest considered Reynolds number. Even for the highest Reynolds number, the natural decrease of a skin friction in turbulent boundary layer is not observed, suggesting that the state of an attached and turbulent boundary layer is not reached in RANS. In the separation bubble, the thicknesses grow, especially the boundary layer thickness and the displacement one. The momentum thickness growth slows down and stagnates before a sudden rise linked to the laminar-turbulent transition leading to turbulence production and boundary layer reattachment. This remarkable point is a source of a slope break for all thicknesses, for both RANS and QDNS results. Nonetheless, a major discrepancy is observed on the displacement thickness as the grow is monotonic for RANS and a thickness decrease is predicted by QDNS, after the maximum of separation bubble thickness. This is the footprint of the mismatch between these two approaches due to turbulence production. This is also visible on the shape factor. The separation is much more massive for RANS than for QDNS, probably due to the lack of turbulence production in RANS computations as previously shown. Moreover, the peak of this integral data is directly linked to the maximum of separation bubble thickness when comparing Figure 8 and Figure 9.

CONCLUSIONS

The previous study (Dufau et al., 2022) showed that a flow feature present in experiments is not captured by QDNS of T106C airfoil. Thus, this investigation aimed at analyzing QDNS carried out at higher Reynolds numbers in order to investigate this hypothesis. The agreement with experimental data is better at higher Reynolds number, especially in the region of the laminar separation bubble characterized by both a static pressure plateau and a strong pressure recovery once the laminar-turbulent transition is triggered. The isentropic Mach number profile close to the trailing edge shows that QDNS is able to capture flow physics of the separation bubble for the high Reynolds numbers. The second objective was the comparison to RANS computations performed with the transition model of Menter and Langtry in order to evaluate it on the T106C configuration. The main discrepancy between these two approaches is the turbulence production once the transition occurred. In QDNS, it is higher and concerns a large part of the boundary layer thickness while, in RANS, the production is smaller and is more influenced by the convection. The boundary layer analysis confirms this statement. Thus, in RANS, the separation is too massive and the size of the bubble is significantly overestimated.

Further works rely on two topics. First, a more deepened study has to be performed to understand the lack of production of turbulence in the RANS simulations. The second topic deals with the effect of the passing wakes on the transition for the T106C cascade. To this end, the experimental configuration with rotating bars will be reproduced by QDNS.

ACKNOWLEDGEMENTS

All RANS simulations have been performed in the framework of the elsA agreement between SAFRAN and ONERA, which are co-owners of this software.

This work was partially granted access to the HPC resources of TGCC Joliot-Curie/Irene and GENCI (allocation A0112A13039).

REFERENCES

Alhawwary, M. A. and Wang, Z. J. (2020). DNS and LES of the flow over the T106C turbine using the high-order FR/CPR method. In *AIAA Scitech 2020 Forum*, page 1572.

Bouchard, M., Marty, J., Deck, S., and Costes, M. (2021). Validation of correlations-based transition modeling strategies applied to the Spalart-Allmaras turbulence model for the computation of separation-induced transition. *Aerospace Science and Technology*, 119:107045.

Cambier, L., Heib, S., and Plot, S. (2013). The Onera elsA CFD Software: Input from Research and Feedback from Industry. *Mechanics & Industry*, 14:159–174.

Dandois, J., Mary, I., and Brion, V. (2018). Large-eddy simulation of laminar transonic buffet. *Journal of Fluid Mechanics*, 850:156–178.

Dufau, A., Marty, J., Man, D., and Piot, E. (2021). Simulation of Passing Wakes Inducing Unsteady Boundary Layer Transition Around Low-Pressure Turbine Blade. In *Turbo Expo: Power for Land, Sea, and Air*, volume 84911. American Society of Mechanical Engineers.

Dufau, A., Marty, J., Man, D., and Piot, E. (2022). High-Fidelity Simulations of the Flow around T106C Cascade at Low Reynolds Number: The Effects of Freestream Turbulence and Stagger Angle. In *Turbo Expo: Power for Land, Sea, and Air*, volume 84911. American Society of Mechanical Engineers.

Garai, A., Diosady, L., Murman, S., and Madavan, N. (2015). DNS of Flow in a Low-Pressure Turbine Cascade Using a Discontinuous-Galerkin Spectral-Element Method. In *Volume 2B: Turbomachinery*. American Society of Mechanical Engineers.

Garai, A., Diosady, L. T., Murman, S. M., and Madavan, N. K. (2016). DNS of low-pressure turbine cascade flows with elevated inflow turbulence using a discontinuous-Galerkin spectral-element method. In *Turbo Expo: Power for Land, Sea, and Air*, volume 49712, page V02CT39A025. American Society of Mechanical Engineers.

Gaster, M. (1967). The structure and behaviour of separation bubbles. *Aeronautical Research Council Reports & Memoranda*.

Gleize, V., Costes, M., and Mary, I. (2021). Numerical Simulation Of NACA4412 Airfoil In Pre-stall Conditions. In *55th 3AF International Conference on Applied Aerodynamics*.

Hillewaert, K., Carton de Wiart, C., Verheylewegen, G., and Arts, T. (2014). Assessment of a high-order discontinuous Galerkin method for the direct numerical simulation of transition at low-Reynolds number in the T106C high-lift low pressure turbine cascade. In *Turbo Expo: Power for Land, Sea, and Air*, volume 45615. American Society of Mechanical Engineers.

Jarrin, N., Benhamadouche, S., Laurence, D., and Prosser, R. (2006). A synthetic-eddy-method for generating inflow conditions for large-eddy simulations. *International Journal of Heat and Fluid Flow*, 27(4):585–593.

Lugrin, M., Beneddine, S., Leclercq, C., Garnier, E., and Bur, R. (2021). Transition scenario in hypersonic axisymmetrical compression ramp flow. *Journal of Fluid Mechanics*, 907.

Marxen, O. and Henningson, D. S. (2011). The effect of small-amplitude convective disturbances on the size and bursting of a laminar separation bubble. *Journal of Fluid Mechanics*, 671:1–33.

Menter, F. R., Langtry, R. B., Likki, S. R., Suzen, Y. B., Huang, P. G., and Völker, S. (2006). A Correlation-Based Transition Model Using Local Variables—Part I: Model Formulation. *Journal of Turbomachinery*, 128(3):413.

Michálek, J., Monaldi, M., and Arts, T. (2012). Aerodynamic Performance of a Very High Lift Low Pressure Turbine Airfoil (T106C) at Low Reynolds and High Mach Number With Effect of Free Stream Turbulence Intensity. *Journal of Turbomachinery*, 134(6).

Plot, S. (2019). The High Level of Maturity of the elsA CFD Software for Turbomachinery Aerodynamics Applications. In *ISABE 2019, Camberra, Australia*, ISABE-2019-24234.

Wilcox, D. C. (1988). Reassessment of the scale-determining equation for advanced turbulence models. *AIAA Journal*, 26(11):1299–1310.